A novel type of insulator-metal transition in non-stoichiometric, amorphous gallium oxide

Lakshmi Nagarajan[1], Roger A. De Souza[1], Dominik Samuelis[1], Ilia Valov[2], Alexander Börger[3], Jürgen Janek[2], Klaus-Dieter Becker[3], Peter C. Schmidt[4] and Manfred Martin[1*]

[1] Institute of Physical Chemistry, RWTH Aachen University, 52056 Aachen, Germany

[2] Institute of Physical Chemistry, Justus Liebig University, 35392 Giessen, Germany

[3] Institute of Physical and Theoretical Chemistry, Technical University of Braunschweig, 38106 Braunschweig, Germany

[4] Institute of Physical Chemistry, Technical University of Darmstadt, 64287 Darmstadt, Germany

* E-mail: martin@rwth-aachen.de

Insulator–metal transitions are well known in transition metal oxides, but inducing an insulator–metal transition in the oxide of a main group element is a major challenge. Here we report the observation of an insulator–metal transition, with a conductivity jump of seven orders of magnitude, in highly non-stoichiometric, amorphous gallium oxide of approximate composition $GaO_{1.2}$ at a temperature around 670 K. We demonstrate through experimental studies and density-functional-theory calculations that the conductivity jump takes place at a critical gallium concentration and is induced by crystallization of stoichiometric Ga_2O_3 within the metastable oxide matrix – in chemical terms by a disproportionation. This novel mechanism — an insulator–metal transition driven by a heterogeneous solid state reaction — opens up a new route to achieve metallic behaviour in oxides that are expected to exist only as classic insulators.

Insulator–metal transitions belong to the most fascinating phenomena in condensed-matter physics[1,2]. Since Mott's landmark work[3,4] it has been known that in crystalline solids strong electron-electron interactions can cause an insulator–metal transition. One example is crystalline Cr-doped vanadium oxide, $(V_{1-x}Cr_x)_2O_3$, which shows a Mott transition from a paramagnetic Mott insulator to a strongly correlated metal upon an increase in pressure, a lowering of temperature, or a decrease in dopant level[5,6]. In non-crystalline solids structural disorder can also lead to an insulator–metal transition on account of Anderson localization[7]. As shown by Anderson[7] and Mott[8], in any non-crystalline material the lowest states in the conduction band are localized, i.e. they are electron traps. Only for energies above the mobility edge, E_c, do states become non-localized or extended. If the Fermi energy E_F is below the mobility edge, states at the Fermi level are localized and the material is an electronic insulator. If, however, the number of electrons increases and the Fermi energy rises above the mobility edge, the material becomes metallic (Anderson transition). As transition metals change their valence state easily, most examples of insulator–metal transitions concern transition metal compounds[4-6,9-11]. The above considerations do not, however, exclude the possibility of inducing an insulator–metal transition in a simple binary oxide of a main group element, even without doping. Instead, large deviations from the ideal stoichiometry, i.e. high defect concentrations, provide a high concentration of electronic defects (self-doping). And if, in addition, the oxide is amorphous, there are two phenomena, strong structural disorder and strong chemical disorder, which could result in an insulator–metal transition.

Here we report such a case: Highly non-stoichiometric, amorphous gallium oxide with an approximate chemical composition $GaO_{1.2}$ shows an unprecedented insulator–metal transition, with a jump in conductivity of ca. 7 orders of magnitude at temperatures as high as 670 K. We show that this insulator–metal transition is chemically induced by an internal redox reaction (a disproportionation), namely the crystallization of stoichiometric β-Ga_2O_3 within the

amorphous oxide matrix, which becomes as a result even more non-stoichiometric. That is, a solid state reaction drives the insulator–metal transition. β-Ga_2O_3 is the only stable oxide of the main group element gallium[12]; it is a stoichiometric compound and a wide gap, n-type semiconductor (optical band gap of 4.9 eV[13]) with applications as a luminescent phosphor[14], as an oxygen sensor[15], or as a deep-UV-transparent oxide[16]. To our knowledge this is the first report on an insulator–metal transition in gallium oxide, perhaps opening up new, potential applications, e.g. in permanent data storage even under severe thermal conditions. In addition, we believe that the novel mechanism, namely the induction of an insulator–metal transition by crystallization of a stoichiometric oxide within a highly non-stoichiometric and amorphous oxide matrix, is not restricted to gallium oxide and thus opens up a new route to reach metallic behaviour in oxides that are expected to exist only as classic insulators.

We prepared highly non-stoichiometric, amorphous gallium oxide starting from targets of β-Ga_2O_3 and depositing the material by means of Pulsed Laser Deposition (PLD) on alumina (0001) single-crystal substrates. The deposition was performed in oxidizing and reducing atmospheres at substrate temperatures between 773 and 873 K. In all cases we find that the as-deposited gallium oxide films are X-ray amorphous. The films differ, however, in their composition and colour. Films prepared in pure oxygen were deposited stoichiometrically, i.e. with a composition Ga:O of 0.40:0.60 as expected for Ga_2O_3, and are transparent. In contrast, the films deposited under reducing conditions (pure argon atmosphere) are highly non-stoichiometric with typical compositions Ga:O of 0.45:0.55, i.e. strong gallium excess, and they are black. The gallium oxides prepared in oxygen are metastable regarding their structure, while the gallium oxides prepared in argon are metastable in two respects, their structure and their chemical composition. We prepared films with thicknesses between 1 and 6 μm. All films have flat surfaces (roughness below 6 nm) and are chemically homogeneous throughout the film thickness (SIMS depth profiling) and also laterally (EPMA line scans).

THE INSULATOR–METAL TRANSITION

At room temperature all as-prepared films are electrical insulators. On heating in an inert atmosphere we observe indeed a pronounced insulator–metal transition for the films prepared in Ar (Fig. 1a). Up to temperatures of about 663 K the conductivity is low ($<10^{-4}$ S cm^{-1}) with a small activation energy of about 0.55 eV (thermal excitation to the mobility edge[4]). At about 663 K the conductivity increases sharply by 7 orders of magnitude and at 673 K the conductivity is already as high as 10^3 S cm^{-1}. During further heating the conductivity decreases again. In contrast, no conductivity jump is found for the amorphous, but stoichiometric gallium oxide, which was prepared in oxygen. Its conductivity is much smaller (inset in Fig. 1a) and increases continuously with increasing temperature with a much higher activation energy of 2.36 eV.

The highly conducting state can be frozen in by quenching the sample to 300 K immediately after the transition. Conductivity measurements for these samples down to temperatures of 5 K (Fig. 1b) show that the conductivity increases during cooling, confirming that the sample in the highly conducting state indeed exhibits metallic behaviour. The conductivity at $T = 5$ K reaches a value as high as $8.6 \cdot 10^3$ S cm^{-1}. Upon subsequent heating in an inert argon atmosphere the high conductivity is retained up to a temperature of 600 K, above which it decreases sharply.

STRUCTURAL INVESTIGATIONS

To obtain insights into the *local* structure of the as-prepared, amorphous gallium oxides we used X-ray absorption spectroscopy at the Ga *K*-edge (Fig. 2a and 2b). Modelling of the extended X-ray absorption fine structure (EXAFS) with FEFF8[17] indicates that the *local* structure around gallium atoms can be described reasonably well by the same oxygen coordination polyhedra as in crystalline β-Ga_2O_3, i.e. strongly distorted oxygen octahedra and

tetrahedra. However, in contrast to β-Ga_2O, which has equal amounts of gallium atoms with octahedral and tetrahedral oxygen coordination, the amorphous, highly non-stoichiometric gallium oxide $Ga_{0.45}O_{0.55}$ contains a significantly higher fraction of gallium atoms with tetrahedral oxygen coordination, Ga_{tet}:$Ga_{oct} \approx 0.57:0.43$ (Fig. 2a, b). The EXAFS results show that the concept of point defects, which is strictly speaking only valid for crystalline structures, should be applicable to our amorphous gallium oxide as well. In this sense, the gallium excess of $Ga_{0.45}O_{0.55}$ compared to β-Ga_2O_3 can be due to gallium interstitials, Ga_I, and/or oxygen vacancies, V_O. Both defects are electron donors, and thus, $Ga_{0.45}O_{0.55}$ can be regarded formally as a heavily donor-doped semiconductor.

To obtain insights into possible structural changes near the insulator–metal transition we employed *in situ* X-ray diffraction. An as-prepared film was heated in an inert atmosphere and X-ray diffractograms were recorded at room temperature (RT), 573 K and then in intervals of 50 K up to 1023 K. The films are X-ray amorphous from RT up to 573 K (Fig. 2c). At 623 K broad peaks appear that can be assigned to β-Ga_2O_3. This means that crystallization of β-Ga_2O_3 starts within the amorphous gallium oxide at least 40 K *below* the insulator–metal transition temperature. High resolution transmission electron microscopy (HRTEM) and selected area electron diffraction (SAED) (Fig. 2d) of a sample that was quenched from T = 673 K to T = 300 K confirm that it consists of a mixture of crystalline β-Ga_2O_3 and an amorphous gallium oxide.

A NOVEL MECHANISM TO INDUCE THE INSULATOR–METAL TRANSITION

The amorphous gallium oxide with gallium excess (gallium interstitials and/or oxygen vacancies) is a heavily donor-doped semiconductor. We expect that the donors form new electronic states above the valence states, thereby decreasing the band gap. As the films prepared in Ar are black in the as-prepared state, the optical band gap is already small enough

for strong optical absorption in the visible and near infra-red range (VIS, NIR) to occur. On the other hand, despite their large gallium excess, our as-prepared samples are insulators, and only during heating to about 673 K do we observe the insulator–metal transition. Thus, the donor concentration in the as-prepared samples is still below the critical donor concentration for closing the band gap. To understand why the donor concentration in the amorphous oxide $Ga_{0.45}O_{0.55}$ increases during heating we recall that about 40 K below the insulator–metal transition temperature crystallization of stoichiometric β-Ga_2O_3 starts (Fig. 2c). This can be described by:

$$Ga_{0.45}O_{0.55}(\text{amorphous}) \longrightarrow Ga_{0.45-2b}O_{0.55-3b}(\text{amorphous}) + b\cdot\beta\text{-}Ga_2O_3(\text{crystalline}) \qquad (1)$$

Here b is the amount of stoichiometric β-Ga_2O_3 that is formed during crystallization. As the formation of β-Ga_2O_3 requires more oxygen than gallium, the gallium excess in the remaining amorphous matrix increases further. Eventually, the donor concentration is driven above the critical value for which the band gap is closed and the amorphous oxide becomes metallic. Equation (1) thus describes an internal redox reaction or a disproportionation that takes place *within* the metastable, amorphous gallium oxide matrix with gallium excess. The high thermodynamic stability of crystalline, stoichiometric β-Ga_2O_3 is the driving force for this internal reaction. No external gas phase oxygen participates in this reaction, as all annealing experiments were conducted in oxygen-free atmospheres.

THEORY

To support our explanation for the observed insulator–metal transition we have calculated the electronic structure of (lattice relaxed) highly non-stoichiometric gallium oxide by means of density functional theory (DFT) using two functionals, GGA[18] and B3LYP[19]. Our DFT

calculations (within the crystal structure P1) show that gallium interstitials, Ga_I, and oxygen vacancies, V_O, both produce defect states in the band gap of Ga_2O_3. For the gallium interstitial we find inside the band gap two new states/bands that are occupied by the three valence electrons of the extra Ga atom (Fig. 3a). These states are localized as can be seen from the charge density plots. For an oxygen vacancy we find a colour centre occupied by two electrons (Fig. 3b). The charge density is highly localized at the oxygen vacancy and the neighbouring Ga ions; more importantly, the states are much closer to the valence band. Consequently, these results strongly suggest that, since we require the band gap to close for the insulator–metal transition, the amorphous phase may be considered more appropriately as containing gallium interstitials (donor states close to the conduction band) rather than oxygen vacancies (donor states close to the valence band). We emphasize, though, that the disproportionation reaction in Eq. (1) does not depend on the nature of the dominating defect.

By increasing the Ga-excess the number of states in the original optical band gap increases and the energy gap between the highest occupied states and the lowest conduction states decreases. This is demonstrated in Fig. 4a where we have plotted the DOS for the supercells $Ga_{20}O_{24}$, $Ga_{22}O_{24}$, and $Ga_{24}O_{24}$ (the composition $Ga_{20}O_{24}$ corresponds to the composition of the as prepared film, $Ga_{0.45}O_{0.55}$). The valence electron states and the defect states start to overlap energetically, the optical band gap decreases from 1.9 eV for $Ga_{20}O_{24}$ to 0.5 eV for $Ga_{24}O_{24}$, and the character of the states in the band gap changes as well. Comparing the charge density distribution of the highest occupied states of $Ga_{24}O_{24}$ (Fig. 4b) with the corresponding density of an isolated Ga_I in Fig. 3a, we see that the states for an isolated Ga_I are much more localized than for highly concentrated Ga_I. This means that with increasing gallium excess the highest occupied states change their character from localized to non-localized electron states. Hence, due to a) the high number of defects, b) the resulting lattice relaxation, and c) the experimental EXAFS results we believe that our calculated

electronic structure describes the essential electronic features of the amorphous oxide in an appropriate way (except for band tailing and the related mobility edges[7,8]). Nevertheless, we cannot predict for two reasons the exact Ga concentration at which the transition from isolating to semi-metallic and metallic behaviour should occur. First, the structure optimization for these systems has been performed assuming triclinic translation symmetry, and second, even for hybrid functionals, such as B3LYP, the calculated band gaps differ from experiment.

NITROGEN DOPING AND OPTICAL ABSORPTION

To provide further experimental support for our hypothesis, we also investigated films deposited in a pure nitrogen atmosphere. Such films contain a small amount of nitrogen and exhibit gallium excess too (typical composition Ga:O:N of 0.47:0.50:0.03); they are also X-ray amorphous. Nitrogen is expected to substitute for oxygen (thus acting as an acceptor and compensating some of the donor defects) and hence it provides us with a means for lowering the Fermi energy. As for the films prepared in argon, we find an insulator–metal transition, but now the conductivity jump is smaller (roughly 5 orders of magnitude) and occurs at higher temperatures ($T \approx 773$ K). Crystallization of β-Ga_2O_3 in the N-doped films starts also at higher temperatures (between 723 K and 773 K) than in films prepared in Ar.

In contrast to films prepared in Ar which are black, as-prepared N-doped films are still transparent, owing to partial compensation of the donors by the acceptor N and the resulting larger optical band gap (as confirmed by DFT). This allows us to further investigate the Ga-O(N) system near the metal-insulator transition by means of *in situ* optical absorption spectroscopy (Fig. 5a). For an as-prepared, N-doped film the optical band gap, $E_g = 3.62$ eV, is smaller than the gap of 4.9 eV in crystalline β-Ga_2O_3 due to the additional states in the band gap (gallium excess) and, in addition, due to band tailing that is caused by the strong chemical

and structural disorder[20]. Upon heating up to T = 773 K only small changes in the absorption spectrum are observed. In contrast, during further heating, shortly above 773 K, the absorption increases rapidly and the film turns completely black. The blackening kinetics (inset in Fig 5a) can be described well by Johnson-Mehl-Avrami kinetics[21], initially with constant nucleation rate of β-Ga_2O_3 and later on with a rate determining step at the interface between the matrix and the growing nucleus. We note that the temperature at which the film becomes black is essentially identical to the insulator–metal transition temperature and slightly higher than the temperature where crystallization of β-Ga_2O_3 starts. As the "blackening" cannot be due to β-Ga_2O_3, which is transparent (band gap 4.9 eV), the remaining amorphous gallium oxide must have become a strong optical absorber.

In summary, the optical absorption experiments confirm that in the as-prepared N-doped gallium oxide the band gap is still too large for optical absorption in the VIS-NIR range, despite the large gallium excess. Crystallization of β-Ga_2O_3 increases the gallium excess in the remaining amorphous matrix and leads to a decreasing band gap that is eventually small enough for complete optical absorption in the VIS-NIR range. Finally, the band gap is closed and the sample exhibits an insulator–metal transition. These results also indicate that by means of doping tuning of the insulator–metal transition temperature is possible.

On heating the blackened film further to 973 K the film becomes again transparent which means that the band gap has opened up again. This de-blackening at elevated temperatures is due to oxidation of the excess gallium in the amorphous part of the film by residual oxygen from the surrounding atmosphere. Once the gallium excess in the amorphous matrix has decreased below the critical value the band gap opens up again resulting in the de-blackening. The first optical spectrum that we were able to measure *in situ* after heating the blackened film to 973 K yields already a small optical band gap, $E_g \approx 1.8$ eV (Fig. 5b). During further de-blackening the optical band gap increases continuously to about 3.6 eV (Fig. 5b) and

eventually the film is again transparent. After long term annealing the band gap approaches the value 4.9 eV for β-Ga_2O_3. The underlying oxidation by residual oxygen from the surrounding atmosphere explains also the strong decrease of the conductivity at elevated temperatures (Fig. 1).

MECHANISM, REVERSIBILITY AND APPLICATIONS

According to the mechanism in Eq. (1), the insulator–metal transition is correlated with a transition from an amorphous oxide of uniform composition to a heterogeneous system that consists of an amorphous oxide and a crystalline oxide of the same element but of different chemical composition. During crystallization of stoichiometric Ga_2O_3 the gallium excess in the amorphous, non-stoichiometric matrix must increase further. If this process is diffusion controlled (diffusion of gallium away from the Ga_2O_3 nucleus and/or diffusion of oxygen towards it) the gallium excess will be highest in the direct vicinity of the nucleus and decrease with increasing distance from the nucleus. Once the critical gallium excess that corresponds to the insulator–metal transition is passed, the Ga_2O_3 nucleus will be surrounded by a shell of metallic gallium oxide. This core-shell structure consists of an insulating Ga_2O_3-core and a metallic, amorphous and highly non-stoichiometric gallium oxide shell that is non-uniform in composition. In the early stage of disproportionation, the metallic shells around the Ga_2O_3 nuclei are not connected, and no percolation of electrons through the metallic regions of the sample is possible. Thus the dc-conductivity is still determined by the connected regions of the amorphous, semiconducting gallium oxide matrix. With increasing time, however, the shells will overlap, and once the percolation threshold is passed, metallic dc-conductivity will be obtained. If, however, the rate determining step is not diffusion but, for example, mass transfer at the interface between the nucleus and the matrix, the amorphous matrix will be characterized by a uniform gallium excess that increases with increasing time. Once the

critical gallium excess that corresponds to the insulator–metal transition is passed the complete amorphous oxide will become metallic, and there will be no percolation phenomenon in the dc-conductivity.

Our experimental results for the Avrami exponents that were obtained from the blackening kinetics (see Fig. 5a) indicate that diffusion is not rate determining. Thus, it seems that percolation does not play a role in this insulator–metal transition. Confirmation of this, however, requires detailed, spatially resolved information from high resolution TEM and electron energy loss spectroscopy (EELS). Summarizing our experimental and theoretical results, our proposed mechanism for the chemically driven insulator–metal transition is displayed schematically in Figure 6. It shows the correlation between the structural changes, the gallium excess in the amorphous oxide, the electrical conductivity, and the band structure.

We close with a few remarks concerning potential applications of the chemically driven insulator–metal transition. For non-volatile storage devices, local laser heating could be used to induce the formation of a Ga_2O_3 nucleus that is surrounded by a small metallic region. Consequently, both differences in conductivity and in optical contrast are large, and could be utilized to store information[22]. In addition, the high thermal stability (up to 300°C, see Fig. 2) would ensure sufficient retention times at room temperature and higher. For re-writable storage devices reversibility is of course required, and the high thermodynamic stability of β-Ga_2O_3 suggests that extreme conditions will be necessary to erase the stored information, i.e. to reverse the crystallization and to homogenize that region. Hence, non-stoichiometric, amorphous gallium oxide may find application in once-write storage devices. For materials systems in which the crystalline, stoichiometric oxide is less stable, reversibility may be reached far more easily, thus making it possible to employ the chemically driven insulator–metal transition in re-writeable storage devices.

METHODS

Gallium oxide films were prepared by Pulsed Laser Deposition with a KrF excimer laser (λ = 248 nm, pulse energy = 200 mJ, Lambda Physik, Germany). Polished sapphire with (0001) orientation was used as substrate. Pellets of Ga_2O_3 (Alfa Aeser, 99.999%) were prepared as target materials. The laser evaporated species were deposited onto the substrates kept at a distance of ~4 cm from the target surface. The deposition was carried out for 45 min at substrate temperatures between 773 and 887 K. Films were deposited in atmospheres of pure oxygen, pure argon or pure nitrogen at a pressure of 4 Pa. The surface morphology of the films was examined with interference microscopy (NT 1100, Veeco Instruments, Germany).

The chemical composition of the films was analyzed by means of Electron Probe Micro Analysis (EPMA) with a CAMEBAX SX 50 (Cameca, France) instrument.

Secondary Ion Mass Spectrometry (SIMS) in depth profiling mode was employed to examine the chemical homogeneity of the films and to confirm the presence of nitrogen in the relevant gallium oxide layers. Depth profiling was performed with a dual beam TOF-SIMS IV (IONTOF GmbH, Germany) instrument[23].

The electrical conductivity of the films was measured in an in-house van der Pauw setup for temperatures between RT and 973 K and a Quantum Design PPMS (Quantum Design, USA) for temperatures between 5K and RT.

X-ray absorption experiments at the Ga *K*-edge were carried out at HASYLAB (Hamburg, Germany) beamline A1, utilizing a Si(311) channel-cut crystal monochromator. Data was acquired in fluorescence geometry with a high-countrate PIPS detector (Canberra). The samples were cooled down to temperatures around 60 K, using a liquid He cryostat (Oxford Instruments). A CoGa alloy (E_0(CoGa) = E_0(Ga) = 10367 eV) was used as an energy reference. All EXAFS data was pre-processed according to the standard procedures[24]. Additionally, all thin film EXAFS spectra were corrected for self-absorption by means of the

Booth and Bridges thin-film correction[25]. The EXAFS data was modelled by fitting with linear combinations of theoretical spectra, that were calculated with FEFF8[17]. One theoretical spectrum for each non-equivalent Ga position of the β-Ga_2O_3 structure (octahedral and tetrahedral coordination of the Ga core) was used. Good fits were obtained with only the octahedral and the tetrahedral contributions to the total spectrum as free parameters. As an indicator for the fit quality, the sum of both weights was checked to be close to unity. Additionally, the validity of our model was verified by fitting EXAFS data of β-Ga_2O_3, and we obtained exactly the expected weights of 0.50±0.04 for both the octahedral and tetrahedral positions of Ga.

In situ X-ray diffraction studies were carried out with Co K_α radiation (λ = 1.7902 Å) in a theta-theta diffractometer (Stoe, Germany) that is equipped with a high temperature chamber (HDK 2.4K, Johanna Otto GmbH, Germany).

High Resolution Transmission Electron Microscopy (HRTEM) and Selected Area Electron Diffraction (SAED) were performed with an analytical transmission electron microscope JEOL JEM 2000 FX II (JEOL, Japan).

In situ optical absorption spectra of the films deposited on Al_2O_3 substrates were recorded with a Lambda-900 Spectrophotometer (Perkin Elmer) in the 250-860 nm wavelength range[26].

We studied the ordering of the electronic states in gallium oxide using density functional theory (DFT) band structure procedures. Isolated point defect were simulated by starting with a supercell of β-Ga_2O_3 , namely $Ga_{64}O_{96}$ and adding one gallium atom, taking out one oxygen atom, or substituting one oxygen atom by nitrogen, respectively. The simulation of higher concentrations of Ga was performed by using a $Ga_{16+n}O_{24}$ supercell. Depending on the property under consideration we used two different variants of DFT, namely (a) the CRYSTAL06 program package[27] with linear combinations of atomic orbitals (LCAO)[28,29] using for Ga, O, and N the basis sets Ga_86-4111d41G_pandey_1994[30,31], O_8-411[32], and

N_6-31d1G[33], respectively, and (b) the Vienna ab initio Simulation Package (VASP) [34] with projector augmented waves (PAW)[35,36.] For the PAWs we used the 3d, 4s and 4p basis functions of Ga, and the 2s and 2p functions of O an N. Structure optimization was performed by the VASP package as VASP is more efficient for structure optimization. The band structure and density of states (DOS) were calculated by both programs, VASP and CRYSTAL. Furthermore we calculated the electronic structure using three different exchange-correlation functionals, namely the GGA approximation with the parameterization of Perdew et al.[18], the GGA+U functional[37], and the orbital dependent exchange functional B3LYP[19]. While GGA renders possible the treatment of a larger number of atoms, it is known to underestimate the band gap[38]. With B3LYP, only smaller systems can be treated, but the calculated band gap is in fair agreement with experimental values[39]. In all calculations the ordering of the states is the same. Only the sizes of the band widths and the band gaps differ for the different functionals.

References

1. Kotliar, G. Driving the Electron over the Edge. *Science* **302**, 67-68 (2003).
2. Erwin, S. C. When is a Metal not a Metal? *Nature* **441**, 295-296 (2006).
3. Mott, N. F. The basis of the electron theory of metals, with special reference to the transition metals. *Proc. Phys. Soc. London Ser. A* **62**, 416-422 (1949).
4. Mott, N. F. *Metal-Insulator Transition* (Taylor & Francis, London, 1974).
5. Mc Whan, D. B. & Remeika, J. P. Metal-insulator transition in $(V_{1-x}Cr_x)_2O_3$. *Phys. Rev. B* **2**, 3734- 3750 (1970).
6. Limelette, P. et al. Universality and Critical Behavior at the Mott Transition. *Science* **302**, 89-92 (2003).

7. Anderson, P. W. Absence of Diffusion in Certain Random Lattices. *Phys. Rev*. **109**, 1492-1505 (1958).
8. Mott, N. F. Electrons in disordered structures. *Adv. Phys.* **16**, 49-144 (1967).
9. Gebhard, F. *The Mott Metal-Insulator Transition* (Springer, Berlin, 1997).
10. Husmann, A. et al. Dynamical Signature of the Mott-Hubbard Transition in $Ni(S,Se)_2$. *Science* **274**, 1874-1876 (1996).
11. Biermann, S., Poteryaev, A. I., Georges, A. & Lichtenstein, A. I. Dynamical singlets and correlation-assisted Peierls transition in VO_2. *Phys. Rev. Lett.* **94**, 026404 (2005).
12. Zinkevich, M. & Aldinger, F. Thermodynamic Assessment of the Gallium-Oxygen System. *J. Am. Ceram. Soc.* **87**, 683-691 (2004).
13. Tippins, H. H. Optical Absorption and Photoconductivity in the Band Edge of β-Ga_2O_3. *Phys. Rev.* **140**, A316-A319 (1965).
14. Binet, L. & Gourier, D. Origin of the blue luminescence of β-Ga_2O_3. *J. Phys. Chem. Solids* **59**, 1241- 1249(1998).
15. Ogita, M., Higo, K., Nakanishi, Y. & Hatanaka, Y. Ga_2O_3 thin film for oxygen sensor at high temperature. *Appl. Surf. Sci.* **175–176**, 721-725 (2001).
16. Orita, M., Ohta, H., Hirano, M. & Hosono, H. Deep-ultraviolet transparent conductive β-Ga_2O_3 thin films. *Appl. Phys. Lett.* **77**, 4166-4168 (2000).
17. Ankudinov, A. L., Ravel, B., Rehr, J. J. & Conradson, S. D. Real-space multiple-scattering calculation and interpretation of x-ray-absorption near-edge structure . *Phys. Rev. B* **58**, 7565-7576 (1998).
18. Perdew, J. P. et al. Atoms, molecules, solids, and surfaces - applications of the generalized gradient approximation for exchange and correlation. *Phys. Rev. B* **46**, 6671-6687 (1992).
19. Becke, A. D. Density-functional thermochemistry 3. The role of exact exchange. *J. Chem. Phys.* **98**, 5648-5652 (1993).

20. Tauc, J. *Amorphous and liquid semiconductors* (Plenum Press, London, 1974).

21. Burke, J. *Kinetics of phase transformations in metals* (Pergamon Press, Oxford, 1965).

22. Wuttig, M., & Yamada, N. Phase change materials for rewriteable data storage. *Nature Mater*. **6**, 824-832 (2007).

23. De Souza, R. A. & Martin, M. Secondary ion mass spectrometry (SIMS) – a powerful tool for studying mass transport over various length scales. *Phys. Stat. Sol. (c)* **4**, 1785-1801 (2007).

24. Koningsberger, D. C. & Prins, R. (Eds.) *X-ray Absorption: Principles, Applications, Techniques of EXAFS, SEXAFS and XANES* (Wiley-Interscience, New York, 1988).

25. Booth, C. H. & Bridges, F. Improved Self-absorption Correction for Extended X-ray Absorption Fine-structure Measurements. *Phys. Scr. T* **115**, 202 (2005).

26. Kreye, M. & Becker, K. D. An optical in-situ study of the re-oxidation kinetics of mixed valent $Yb_3Al_5O_{12}$. *Phys. Chem. Chem. Phys.* **5**, 2283-2290 (2003).

27. Dovesi, R. et al. *CRYSTAL06 User's Manua* (University of Torino, Torino, 2006).

28. Bloch, F. Über die Quantenmechanik der Elektronen in Kristallgittern. *Z. Physik* **52**, 555-600 (1928).

29. Slater, J. C. & Koster, G. F., Simplified LCAO method for the periodic potential problem. *Phys. Rev.* **94**, 1498-1524 (1954).

30. Pandey, R., Jaffe, J. E. & Harrison, N. E. Ab-initio study of high-pressure phase-transition in GaN. *J. Phys. Chem. Solids* **55**, 1357-1361 (1994).

31. Pandey, R., Causa, M., Harrison, N. M. & Seel, M. The high-pressure phase transitions of silicon and gallium nitride: A comparative study of Hartree-Fock and density functional calculations. *J. Phys. Cond. Matter* **8**, 3993-4000 (1996).

32. Bredow, T., Jug, K. & Evarestov, R. A. Electronic and magnetic structure of $ScMnO_3$. Phys. Status Solidi (b) 243, R10-R12 (2006).

33. Gatti, C., Saunders, V. R. & Roetti, C. Crystal-field effects on the topological properties of the electron-density in molecular-crystals - the case of urea. *J. Chem. Phys.* **101**, 10686-10696 (1994).

34. Kresse, G. & Furthmuller, J. VASP the guide, http://cms.mpi.univie.ac.at/vasp/vasp/vasp.html

35. Blöchl, P. E. Projector augmented-wave method**.** *Phys. Rev. B* **50**, 17953-17979 (1994).

36. Kresse, G. & Joubert, J. From ultrasoft pseudopotentials to the projector augmented-wave method. *Phys. Rev. B* **59**, 1758-1775 (1999).

37. Anisimov, V. I., Zaanen, J. & Andersen, O. K. Band theory and Mott insulators - Hubbard-U instead of Stoner-I. *Phys. Rev. B* **44**, 943-954 (1991).

38. Goodby, R. W., Schlüter, M. & Sham, L. J. Trends in self-energy operators and their corresponding exchange-correlation potentials. *Phys. Rev. B* **36**, 6497-6500 (1987).

39. Muscat, J., Wander, A. & Harrison, N. M. On the prediction of band gaps from hybrid functional theory. *Chem. Phys. Lett.* **342**, 397-401 (2001)

Acknowledgements

We gratefully acknowledge support by the Deutsche Forschungsgemeinschaft (DFG) within the Priority Program 1136. We thank J. Rodesch for performing preliminary measurements; R. Dronskowski allowing us to use the Quantum Design PPMS ; HASYLAB for the provision of beam time and travel funding; E. Welter, W. Calibe, J. Brendt, D. Müller, and D. Röhrens for support during the XAS measurements; and T. Weirich for the TEM measurements.

Correspondence and requests for materials should be addressed to M. M.

Figure Legends

Figure 1 Electrical conductivity of gallium oxide films prepared by PLD.

a, Conductivity as a function of temperature for three films (■, ■, ■) which were prepared under reducing conditions in an argon atmosphere. Below the insulator–metal transition temperature, $T_{IM} \approx 663$ K, the films exhibit semiconducting behaviour (fitted solid lines and corresponding activation energies, E_a). The inset shows the conductivity (▲) of a film prepared under oxidizing conditions in pure O_2. **b**, Conductivity of a gallium oxide film, that was prepared in Ar, heated quickly to T = 673 K, which is just above the insulator–metal transition temperature, and quenched subsequently to T = 300 K. During cooling from T = 300 K to T = 5 K and subsequent heating to T = 300 K (◆) the conductivity was measured with a PPMS device. During further heating to T = 745 K (▷) the conductivity was measured with a van der Pauw setup.

Figure 2 Structure of gallium oxide films, $Ga_{0.45}O_{0.55}$, prepared by PLD in argon atmosphere.

a, EXAFS, $k^2 \cdot \chi(k)$, of an as-prepared, amorphous gallium oxide film at the Ga *K*-edge. **b**, Modified radial distribution function $G'(R)$ (Fourier transform of the EXAFS in panel a). The fit (blue lines) of the experimental data (black lines) with a linear combination of theoretical spectra for gallium atoms with tetrahedral surrounding, Ga_{tet}, and octahedral surrounding, Ga_{oct}, yields a distribution Ga_{tet} : Ga_{oct} = (0.57±0.03) : (0.43±0.03). **c**, The as-prepared film was heated in an inert atmosphere and *in situ* X-ray diffractograms were taken. Up to 573 K the film is X-ray amorphous. Starting from 623 K broad diffraction peaks appear which we assign to β-Ga_2O_3. The small shift of

the experimental peak positions relative to the powder pattern of β-Ga_2O_3 at the bottom of the figure (JCPDS 87-1901) is due to slight changes of the diffraction geometry during heating. **d,** Cross-sectional high-resolution transmission electron microscopy (HRTEM) picture of a film that was annealed at 673 K and then quenched to 300 K, showing a sharp interface between the alumina substrate and the gallium oxide film. The inset displays a selected area electron diffraction pattern (SAED) of the gallium oxide film. The d-spacings calculated from the diffraction peaks and the diffuse background confirm that the film consists of a mixture of crystalline β-Ga_2O_3 and an amorphous gallium oxide.

Figure 3 Density of states (DOS) and electron density distribution for gallium oxide with small gallium excess.

Isolated defects were considered by starting with a supercell of β-Ga_2O_3, namely $Ga_{64}O_{96}$ and adding one gallium atom (gallium interstitial Ga_I) or taking out one oxygen atom (oxygen vacancy V_O). Due to the large number of atoms the GGA functional was used in the DFT calculations. In the DOS plots the states from the top of the O 2p like valence states to the lowest conduction states are displayed (occupied states are coloured). Within the band gap we find the defect states, for which the corresponding electron density distribution is also displayed (red = highest electron density). **a**, Gallium interstitial, $Ga_{64}Ga_IO_{96}$: The 3 valence electrons of Ga_i occupy the states in the band gap at $E - E_F \approx -1$ eV and at $E - E_F = 0$ eV. These states are localized (covalent bonds of the interstitial Ga to the neighbouring O and the nearest neighbour Ga) as can be seen from the coloured charge density plots which are shown for two lattice planes. The Ga_I is located in the centre of the upper plane. **b**, Oxygen vacancy, $Ga_{64}O_{95}V_O$: The oxygen vacancy V_O produces a defect state at

E - E_F = 0 eV, close to the valance band. The defect state is occupied by two electrons (colour centre). The corresponding electron density is highly localized at the oxygen vacancy and (to a much lesser extent) also at the neighbouring two Ga ions.

Figure 4 Electronic structure of supercells $Ga_{20}O_{24}$, $Ga_{22}O_{24}$, and $Ga_{24}O_{24}$.

a, Density of states (DOS) calculated with the B3LYP functional. The states from the O 2p like valence states to the bottom of the conduction bands are displayed. The occupied states are coloured (light = valence states, dark = defect states). The energy gap between the valence states and the unoccupied states in the conduction band is ≈ 4.5 eV (see DOS of $Ga_{20}O_{24}$), in fair agreement with the experimental value of 4.9 eV for β-Ga_2O_3 (as expected for the functional B3LYP) **b**, Electron density distribution of the uppermost occupied defect states of Ga_I in $Ga_{24}O_{24}$ (states at $E \approx$ -0.5 eV in panel a) for two lattice planes. Ga_I is located in the lower plane and at these concentrations of Ga_I the character of the defect states changes from localized to non-localized.

Figure 5 *In situ* optical absorption of a gallium oxide film deposited in nitrogen.

The quantity $(A \cdot h\nu)^2$ is plotted against the energy (A = absorption, $h\nu$ = photon energy). The intercept of the tangent at high energies with the energy axis yields the optical band gap E_g [20]. **a**, Optical absorption spectra were taken during heating from RT to 773 K. The optical band gap at RT is E_g = 3.62 eV. Only slight changes in the absorption are observed during heating. To follow the kinetics of the blackening process, we heated an as-prepared sample rapidly to 793 K and measured at this temperature the absorbance, A, at a fixed wavelength of 800 nm as function of time

(inset in Fig. 5a, black symbols). We find a fast increase of *A* and saturation after about 20 min. The blackening kinetics is described well by Johnson-Mehl-Avrami kinetics[21], $A(t) = A_{max} \cdot (1 - \exp(-(kt)^n))$ (red line). The exponent *n* is initially 4 (constant nucleation rate of β-Ga_2O_3) and changes after about 800 s to 3 (rate determining step at the interface between the matrix and the growing precipitate), while the rate constant *k* changes only slightly from $k = 3.5 \cdot 10^{-4}$ s^{-1} to $k = 7 \cdot 10^{-4}$ s^{-1}. **b,** Optical absorption spectra taken as a function of time after blackening at 793 K (panel a) and subsequent fast heating to 973 K. The band gap opens up again resulting in de-blackening of the film. The first spectrum that could be measured yields a gap of 1.81 eV, and with increasing time the gap increases to 3.61 eV.

Figure 6 Schematic description of the correlation between geometrical structure, gallium excess, electrical conductivity, and band structure of highly non-stoichiometric, amorphous gallium oxide as a function of temperature.

The scheme summarizes our experimental and theoretical findings. It also demonstrates that the insulator–metal transition is correlated with a transition from an amorphous oxide of uniform composition to a heterogeneous system that consists of an amorphous oxide and a crystalline oxide of the same element, but of different chemical composition.

a, The as- prepared gallium oxide with gallium excess, $GaO_{1.2}$, is amorphous with a short range order where Ga (blue) is tetrahedrally and octahedrally coordinated by oxygen (red) (as determined by EXAFS). The depicted geometrical structure is a schematic, two-dimensional cut through the amorphous structure. The conductivity is low with a small activation energy corresponding to the gap (lower row) between the defect states (gallium excess) and the conductivity band (or the mobility edge). **b,** At

the temperature T_{cryst} nucleation and growth of crystalline, stoichiometric β-Ga_2O_3 (white nucleus) starts (as determined by *in situ* XRD and *in situ* optical spectroscopy), resulting in an increasing gallium excess in the remaining amorphous oxide. Due to the increasing Fermi energy, E_F, and the decreasing band gap the conductivity increase is now steeper than below T_{cryst}. **c**, At the temperature T_{IM} a critical number of β-Ga_2O_3 nuclei and a critical gallium excess in the remaining amorphous gallium oxide is reached; the band gap is closed and the conductivity jumps by seven orders of magnitude (insulator–metal transition). Based on the Avrami exponents (blackening kinetics in Fig. 5a) growth of the β-Ga_2O_3 nuclei is not diffusion controlled, and thus the insulator–metal transition within the amorphous gallium oxide proceeds homogeneously, as indicated by the uniform colouring in the top row.

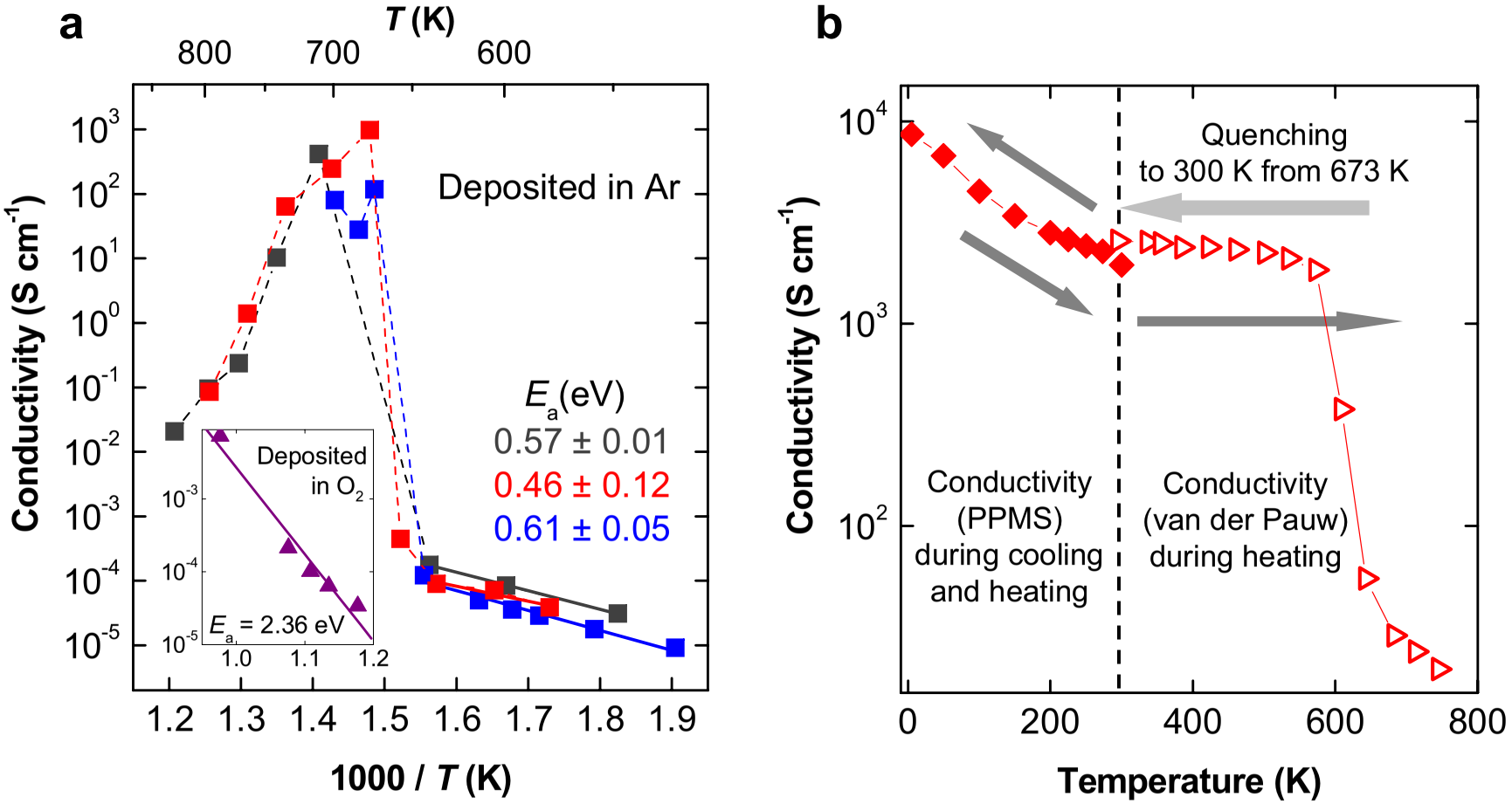

Figure 1 Electrical conductivity of gallium oxide films prepared by PLD.

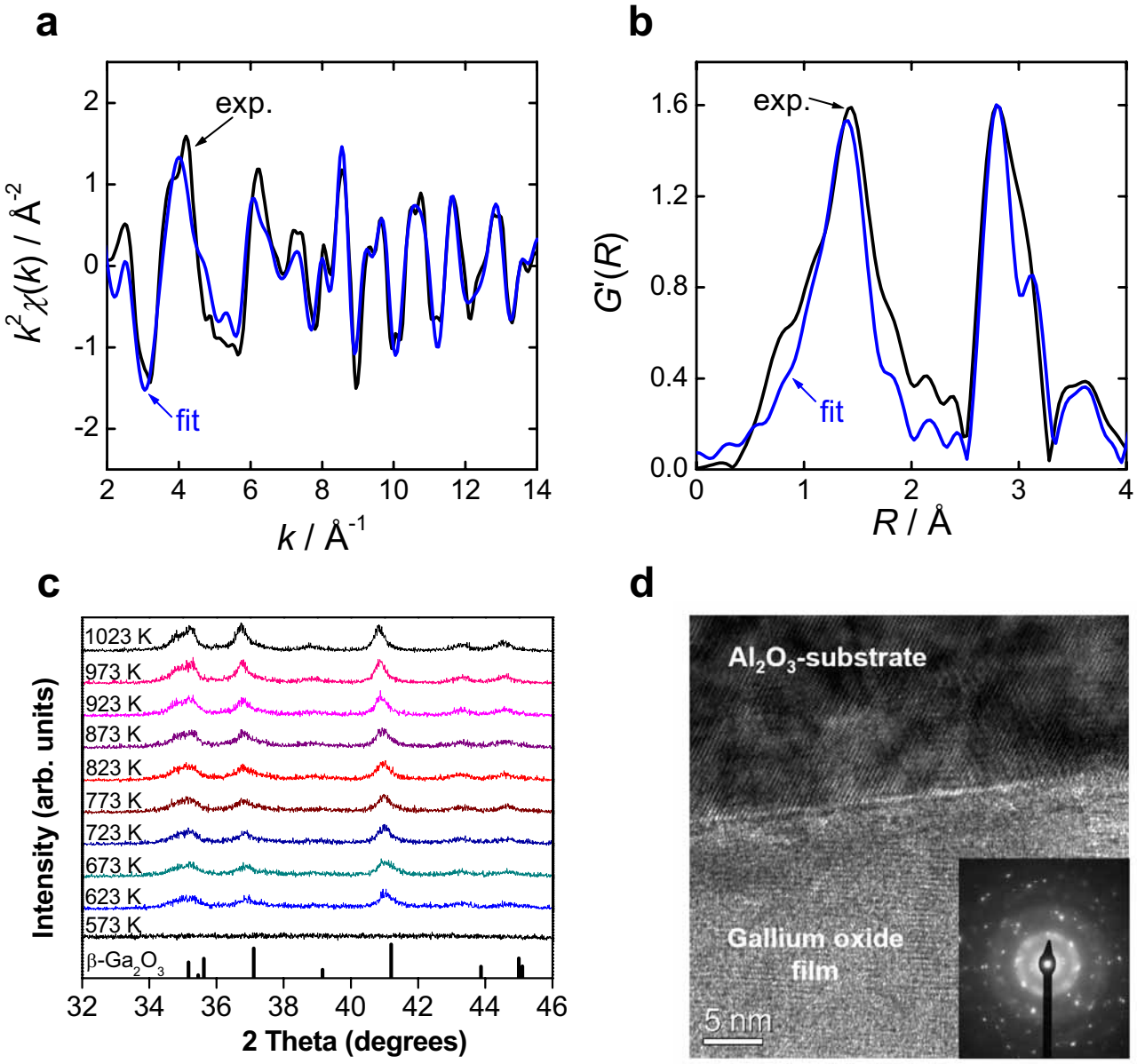

Figure 2 Structure of gallium oxide films, $Ga_{0.45}O_{0.55}$, prepared by PLD in argon atmosphere.

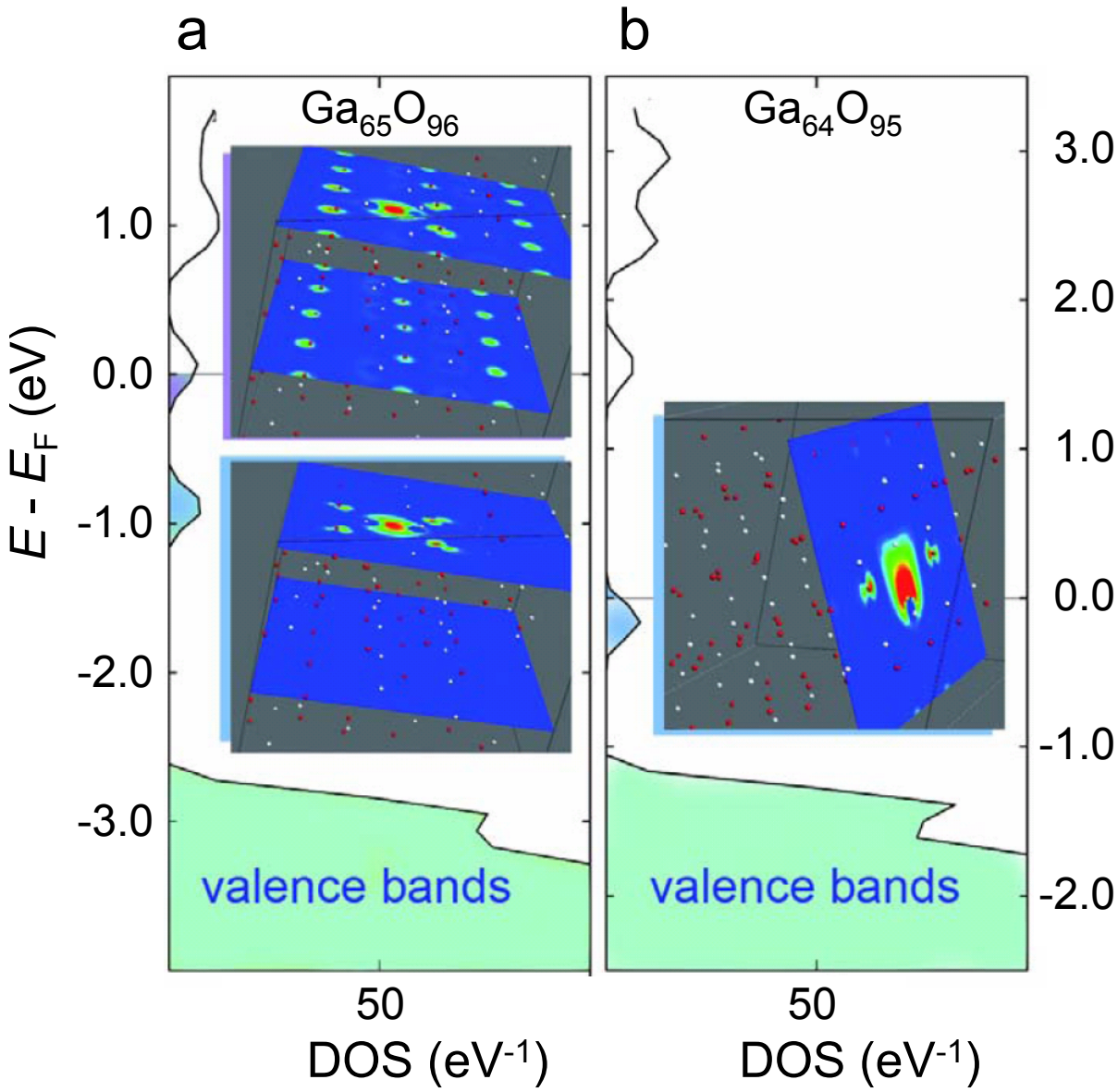

Figure 3 Density of states (DOS) and electron density distribution for gallium oxide with small gallium excess.

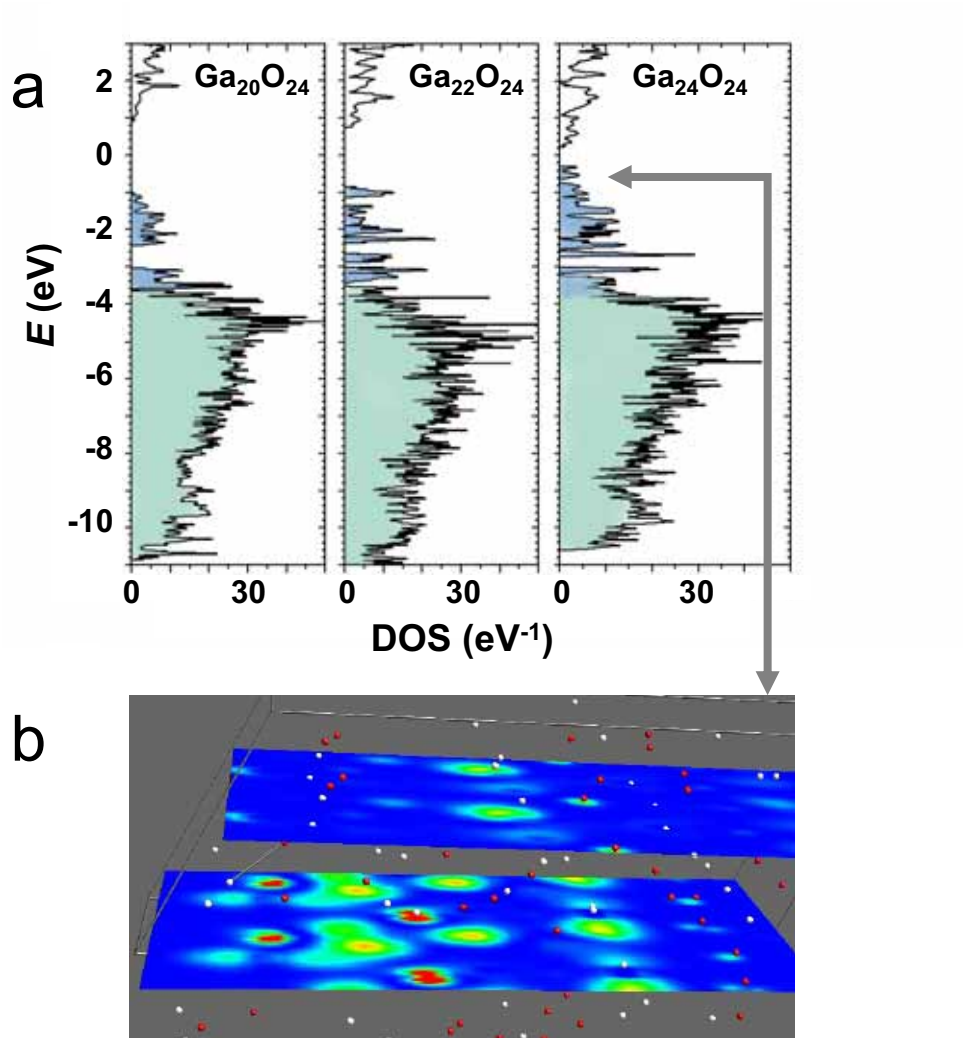

Figure 4 Electronic structure of supercells $Ga_{20}O_{24}$, $Ga_{22}O_{24}$, and $Ga_{24}O_{24}$.

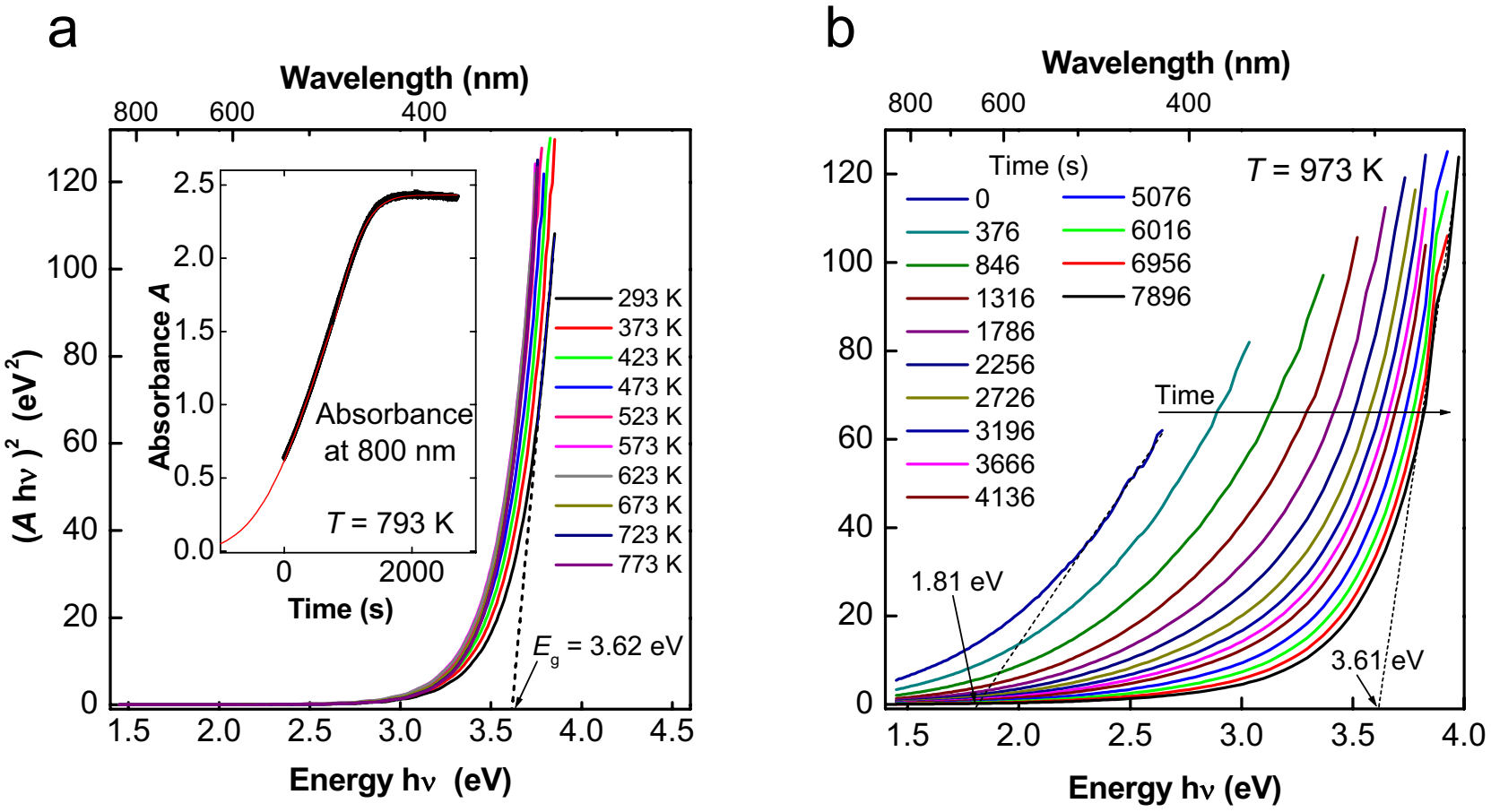

Figure 5 *In situ* optical absorption of a gallium oxide film deposited in nitrogen.

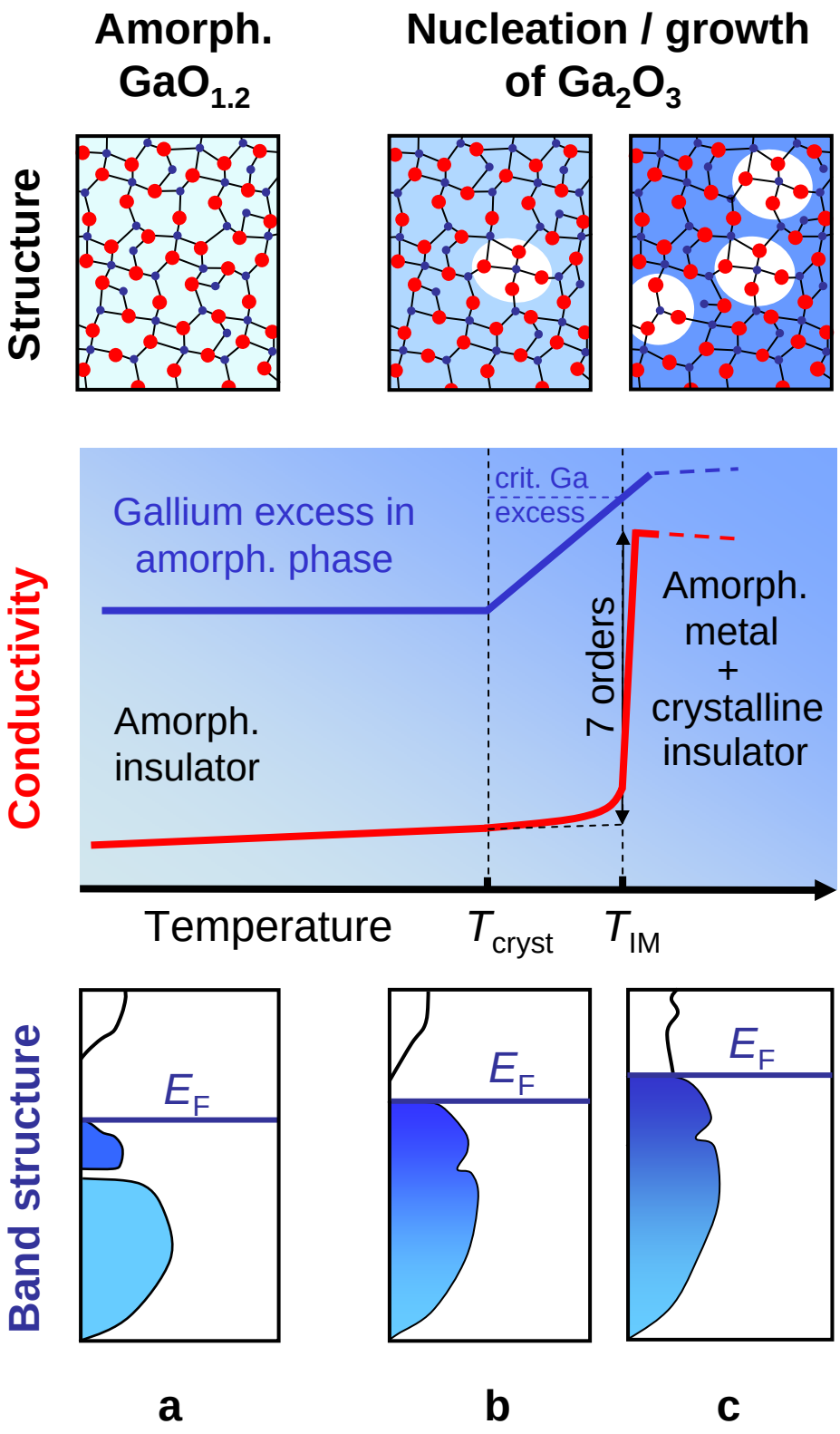

Figure 6 Schematic description of the correlation between geometrical structure, gallium excess, electrical conductivity, and band structure of highly non-stoichiometric, amorphous gallium oxide as a function of temperature.